Ultra-sensitive high-precision spectroscopy of a fast molecular ion beam

Andrew A. Mills, Brian M. Siller, Michael W. Porambo, Manori Perera, Holger Kreckel et al.

Related Articles

Molecular-beam study of the ammonia–noble gas systems: Characterization of the isotropic interaction and insights into the nature of the intermolecular potential
J. Chem. Phys. 135, 194301 (2011)

An LIF characterization of supersonic BO (X2+) and CN (X2+) radical sources for crossed beam studies
Rev. Sci. Instrum. 82, 083107 (2011)

On the rotational temperature and structure dependence of electric field deflection experiments: A case study of germanium clusters
J. Chem. Phys. 135, 034303 (2011)

Theory of the optical spatial separation of racemic mixtures of chiral molecules
J. Chem. Phys. 132, 194315 (2010)

Specific formation of negative ions from leucine and isoleucine molecules
J. Chem. Phys. 132, 014301 (2010)

Additional information on J. Chem. Phys.

Ultra-sensitive high-precision spectroscopy of a fast molecular ion beam

Andrew A. Mills,[1] Brian M. Siller,[1] Michael W. Porambo,[1] Manori Perera,[1,a)]
Holger Kreckel,[1] and Benjamin J. McCall[1,2,b)]
[1]*Department of Chemistry, University of Illinois, Urbana, Illinois 61801, USA*
[2]*Departments of Physics and Astronomy, University of Illinois, Urbana, Illinois 61801, USA*

Direct spectroscopy of a fast molecular ion beam offers many advantages over competing techniques, including the generality of the approach to any molecular ion, the complete elimination of spectral confusion due to neutral molecules, and the mass identification of individual spectral lines. The major challenge is the intrinsic weakness of absorption or dispersion signals resulting from the relatively low number density of ions in the beam. Direct spectroscopy of an ion beam was pioneered by Saykally and co-workers in the late 1980s, but has not been attempted since that time. Here, we present the design and construction of an ion beam spectrometer with several improvements over the Saykally design. The ion beam and its characterization have been improved by adopting recent advances in electrostatic optics, along with a time-of-flight mass spectrometer that can be used simultaneously with optical spectroscopy. As a proof of concept, a noise-immune cavity-enhanced optical heterodyne molecular spectroscopy (NICE-OHMS) setup with a noise equivalent absorption of $\sim 2 \times 10^{-11}$ cm^{-1} Hz$^{-1/2}$ has been used to observe several transitions of the Meinel 1–0 band of N$_2^+$ with linewidths of $\sim$120 MHz. An optical frequency comb has been used for absolute frequency calibration of transition frequencies to within $\sim$8 MHz. This work represents the first direct spectroscopy of an electronic transition in an ion beam, and also represents a major step toward the development of routine infrared spectroscopy of rotationally cooled molecular ions. © *2011 American Institute of Physics.* [doi:10.1063/1.3665925]

I. INTRODUCTION

The study of molecular ions is important in a number of fields, including physical chemistry, combustion chemistry, atmospheric chemistry,[1] and astrochemistry.[2,3] Ions are transient and reactive species, so even in plasma discharges, neutral molecules are typically $\sim$6 orders of magnitude more abundant than the ions of interest. Early spectroscopic studies on glow discharges were often hampered by interfering signals from neutral absorbers.[4] The invention of velocity modulation spectroscopy (VMS),[5] which involves using a high voltage AC discharge to modulate the velocity of ions and a lock-in amplifier to isolate the modulated ionic absorption signals from the unmodulated neutral signals, has allowed for the spectroscopic study of scores of molecular ions.[4] However, due to harsh plasma conditions, molecular ions produced in VMS experiments often have high rotational and vibrational temperatures, typically on the order of several hundred Kelvin. For example, CH$_3^+$ has been studied by Oka and co-workers in a liquid nitrogen cooled discharge cell, where the rotational and vibrational temperatures were reported as 371 and 700 K, respectively.[6]

Until recently,[7] all VMS experiments produced Doppler-limited linewidths. For small diatomic molecules, the spectra remain relatively simple to assign and line intensities are fairly strong, but larger (e.g., C$_3$H$_3^+$) or highly fluxional (e.g., CH$_5^+$) molecular ions are more challenging targets, as each individual transition is weaker due to quantum dilution. Supersonically expanding discharges have been used to spectroscopically study rotationally cold molecular ions, but the reduced rotational temperature comes with the price of lost ion/neutral discrimination. Although concentration modulation can provide some discrimination from background precursors,[8] radicals[9] and excited states of stable neutrals can still congest and complicate the recorded spectrum.

The limitations of current techniques are highlighted by the case of CH$_5^+$, a molecular ion of considerable interest due to its lack of a classical structure[10] and as the prototypical non-classical carbocation.[11] The only published high-resolution spectrum of CH$_5^+$ was recorded by Oka and co-workers[12] in a liquid nitrogen cooled discharge of H$_2$ and CH$_4$, and was identified by a process of elimination, by removing the known spectral lines of H$_3^+$, CH$_3^+$, C$_2$H$_3^+$, HCO$^+$, HCNH$^+$, the Rydberg spectrum of H$_2$, and strong lines of CH$_4$ that remained due to a slight asymmetry in the AC plasma. This rich spectrum ($\sim$900 lines, due to the fairly high rotational temperature) may still contain some transitions of other ions, and almost certainly is missing some CH$_5^+$ transitions due to overlap with CH$_4$ lines. As a result of the complexity of the spectrum, it remains completely unassigned more than a decade since its publication.

Nesbitt and co-workers have recorded[13] a spectrum of a supersonically expanding H$_2$:CH$_4$ plasma, the broad outline of which has been published.[14] Their spectrum evidently

a)Present address: Department of Chemistry, Illinois Wesleyan University, Bloomington, Illinois 61702, USA.
b)Author to whom correspondence should be addressed. Electronic mail: bjmccall@illinois.edu.

contains not only many transitions that coincide with those of Oka and co-workers, but also many transitions that do not. Because of the lack of a rigorous ion/neutral discrimination, it is possible that some of these transitions may be due to excited CH_4. They have proposed[13] the use of four-line combination differences to help assign the spectrum, but this effort requires higher precision in the determination of line centers.[15]

The ideal experiment for studying the spectra of complex ions such as CH_5^+ may be a combination of a supersonic expansion ion source with fast ion beam spectroscopy. This approach offers rigorous ion/neutral discrimination (by physically separating ions from neutrals) and reduced Doppler linewidths (from kinematic compression), and also allows mass identification of each spectral line (from Doppler splittings).

Although action spectroscopy of ion beams was successfully implemented as early as the 1970s (Ref. 16), the only direct ion beam spectrometer (prior to the present work) was developed in the late 1980s by Saykally and co-workers at Berkeley.[17] This instrument was successfully used to measure the mid-IR absorption spectra of HF^+, HN_2^+, HCO^+, H_3O^+, and NH_4^+ (Refs. 17–19), but was abandoned after a few years, as it did not have sufficient sensitivity to pursue the spectra of the larger and fluxional ions they were most interested in, given the rotational temperature of uncooled ion sources.

With an eye to applications such as CH_5^+, we have embarked on an effort to construct a second-generation direct ion beam spectrometer, which incorporates a number of technological advances from the past two decades and is also designed to be fed with a continuous supersonic expansion discharge source.[20] As this approach will combine ultra-high sensitivity, rotational cooling, and very high precision line center determination, we refer to it as sensitive, cooled, resolved ion beam spectroscopy (SCRIBES).

This paper describes an important step toward SCRIBES, in the form of a new ion beam instrument that uses a Ti:Sapphire laser (the future pump laser for a mid-IR difference frequency laser) in concert with NICE-OHMS[21] as a sensitive direct spectroscopic probe of the ion beam. This instrument uses a time-of-flight mass spectrometer (TOF-MS) to provide mass analysis of constituents of the ion beam at spectroscopically relevant beam energies. An optical frequency comb is used to accurately and precisely measure the frequencies of the observed transitions.

The initial proof of concept system studied in this work is the 1–0 band of the $A^2\Pi_u - X^2\Sigma_g^+$ Meinel system of N_2^+, which is an important species in atmospheric aurorae and electrical discharges. Because the line centers of many transitions in this band have already been measured at Doppler-limited resolution,[22] N_2^+ serves as a useful benchmark of the capabilities of our fast ion beam spectrometer.

II. EXPERIMENTAL

A. Overview

Figure 1 shows an overview of the entire experimental setup, which can be divided into two functional groups: (1) the ion beam setup, including the ion source, the ion optics

and the mass spectrometer; and (2) the spectroscopic setup, consisting of the laser system and signal detection electronics. The two parts of the system interact in the central overlap region, where the laser cavity and the ion beam are superimposed.

In order to minimize vibrations in the spectroscopic setup, the optical components are mounted on a pneumatically stabilized laser table that is mechanically isolated from the ion beam setup. The mirrors of an optical cavity (finesse $\mathcal{F} \sim 450$) are positioned on breadboards that overhang the edge of the laser table and surround the ion beam drift region. Within the optical cavity, the laser is coupled through Brewster windows mounted on the ion beam chamber, and is overlapped with the ion beam within the drift region.

A cold cathode ion source, described in detail in Sec. II B, is used to produce a beam of N_2^+ at energies ranging from 2–6 kV. After the beam is extracted from the source, it is focused by an Einzel lens and steered by two sets of parallel electrostatic plates into a cylindrical electrostatic double-focusing deflector.[23] When this deflector is biased, the ion beam is turned 90° and focused into the drift tube. When the deflector plates are grounded, the ion beam proceeds straight through a hole in the outer deflector plate and into a Faraday cup that is used to optimize source conditions for maximum ion current, which is generally ~ 10 μA.

After exiting the deflector chamber, the ion beam proceeds through a 27 cm long drift tube and two metal plates that are spaced 13 cm apart, centered in the drift region. The metal plates are attached to vertical linear manipulators; each plate has three 3-mm diameter apertures that are spaced 1.5 cm vertically and 1 mm horizontally. The apertures are aligned with the laser horizontally by choosing the hole that does not spoil the cavity finesse, and vertically within a hole by fine-tuning the vertical translation of the plates. After the appropriate apertures are centered on the laser, the ion beam is steered through the same apertures to make the laser and the ion beam collinear. The drift tube and the aperture plates are all electrically isolated from the surrounding chamber and connected to one another so they can all be used to modulate the velocity of the ion beam with an applied voltage. After the drift region, the ion beam enters the second 90° bender which guides the ions out of the laser cavity into the time-of-flight mass spectrometer, which is described in detail in Sec. II D.

Optical spectroscopy of the ion beam is performed using the NICE-OHMS[21] technique, which combines the long effective path length of cavity enhanced spectroscopy with the noise suppression of heterodyne spectroscopy. Further noise suppression is obtained by modulating the velocity of the ions by applying a square wave voltage to the drift tube. A more thorough description of the detection system is given in Sec. II E.

B. Ion source

Our instrument is engineered to accommodate a continuous supersonic expansion discharge source, such as the one we have previously characterized for H_3^+ spectroscopy.[20] To utilize such a source, our ion source chamber was designed
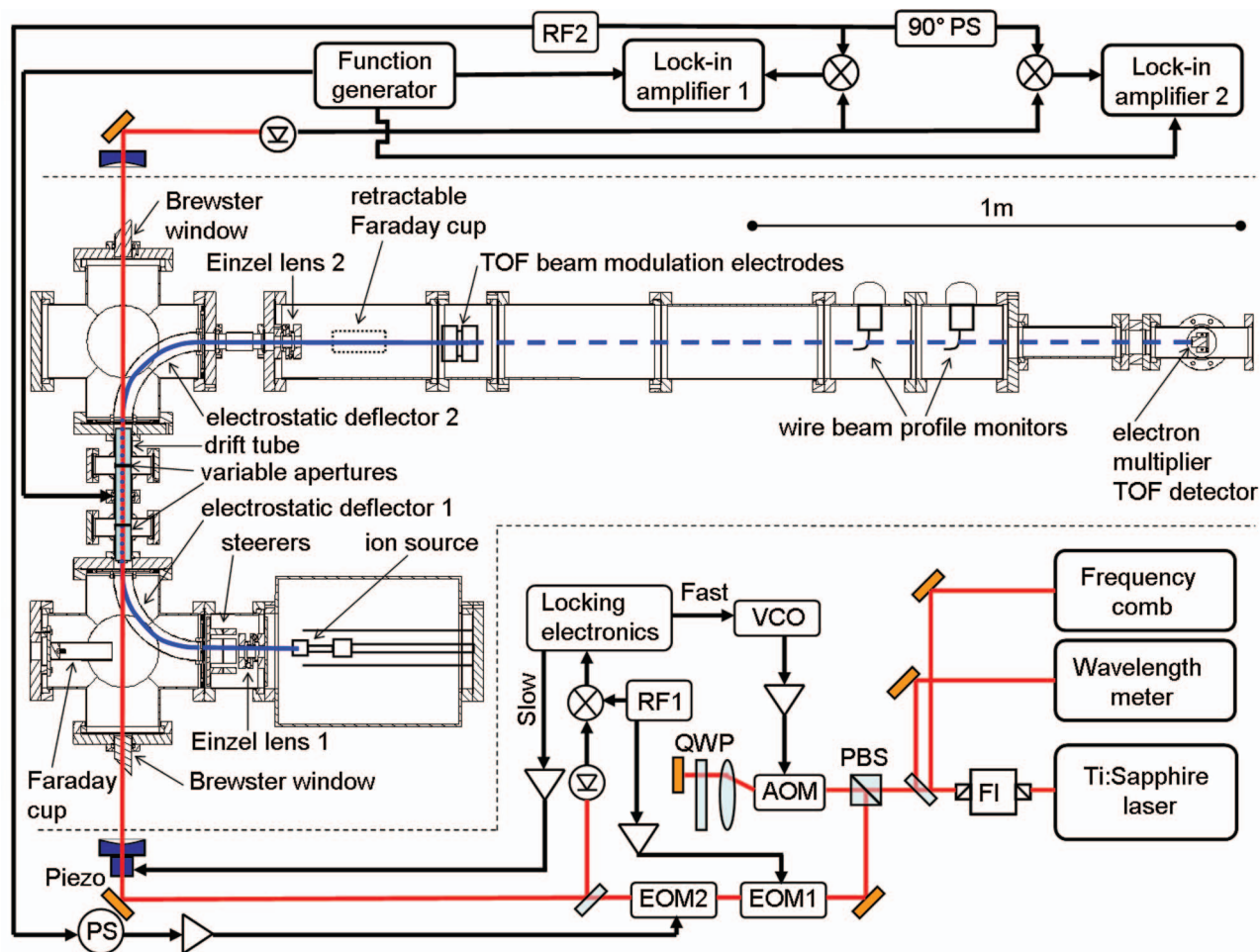
FIG. 1. Schematic of the fast ion beam spectrometer using NICE-OHMS detection. The following abbreviations are used: Faraday isolator (FI), polarizing beam splitter (PBS), double pass acousto optic modulator (AOM), quarter wave plate (QWP), electro optic modulator (EOM), radio-frequency synthesizer (RF), voltage controlled oscillator (VCO), phase shifter (PS), and time-of-flight (TOF). Amplifiers are indicated with triangles.

to be large in size, and to couple to a high-throughput Roots pumping system through large-diameter tubing. However, for the initial testing of the instrument described here, we have designed a modular cold cathode discharge source for simplicity.

Our cold cathode source was made with a fused silica tube held by two electrodes, with an opening at the back for sample gas inlet, and another at the front through which ions are extracted. The electrodes are constructed using stock Ultra-Torr (Swagelok) unions. High temperature silicone O-rings are used to make seals to the fused silica tube which has ground-polished ends. The front electrode uses a custom modified ferrule with a 1 mm diameter aperture to allow ions to be extracted, and a 22° bevel to reduce beam expansion induced by space-charge interaction.[24, 25] A small circle of stainless steel mesh was used in the back electrode to produce a more uniform electric field while still allowing gas to flow through the inlet. This source has proven to be robust, operating for typically 40 hrs before the front ferrule needs to be cleaned and the fused silica tube interchanged.

A schematic view of the source and its electrical connections is shown in Figure 2. An aluminum cap holds the back electrode to provide mechanical stability and allow for electrical and water-cooling connections. The ions are extracted

through a 0.25" diameter hole in a grounded stainless steel plate after the front electrode.

The front electrode (cathode) is biased to 2–6 kV by the "float power supply," which determines the ion beam voltage. The rear electrode (anode) is biased to an additional 3.5 kV above the beam voltage by the "discharge power supply," the ground of which is floated to the beam voltage by the float power supply. The discharge supply is powered through an isolation transformer, and fully enclosed in a polycarbonate box for safety.
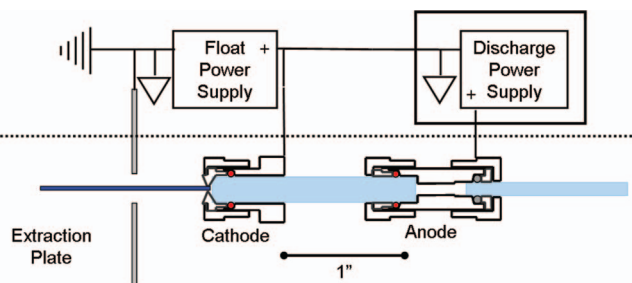

FIG. 2. A schematic of the cold cathode source and its electrical connections. Gas flows in from the right, and ions are extracted to the left. In this figure, the triangles indicate the "ground" connections of the power supplies; the polycarbonate isolation box for the discharge power supply is also indicated.

C. Ion optical system

The vacuum system, with the exception of the ion source chamber, is made from standard stainless steel Conflat components in order to achieve high vacuum conditions. The homebuilt ion source chamber, which is designed with a high-throughput expansion source in mind, is currently pumped by a 2000 L/s turbomolecular pump and has a pressure of $\sim 5 \times 10^{-6}$ Torr during operation.

The overlap and mass spectrometry regions are pumped by two 500 L/s turbomolecular pumps situated below the 90° deflector chambers, establishing typical pressures during operation of 6×10^{-7} Torr at deflector 1 and 8×10^{-8} Torr at deflector 2. The vacuum cross that houses the mass spectrometer detector is pumped by a 250 L/s turbomolecular pump, and has a typical pressure of $\sim 2 \times 10^{-8}$ Torr.

The ion optical configuration was designed to optimize the ion density in the laser/ion overlap region between the two electrostatic deflectors. All ion optical elements are electrostatic, so all particles with the same kinetic energy and charge state are guided on the same trajectory regardless of particle mass. The positive ions that emerge from the ion source with a voltage V_{beam} are initially focused by the first Einzel lens. In the next short vacuum nipple, the ion beam traverses a set of two parallel plate steerers. Each set of steerers can be used to deflect the ion beam both horizontally and vertically, allowing for an adjustment of the beam angle as well as for parallel offsets to the ion beam position. Each steerer plate is supplied by an independent bipolar power supply with voltages up to ± 1000 V. By applying voltages of the same sign to opposing steerer plates, it is also possible to induce additional horizontal or vertical focusing in the steerer section.

The cylindrical 90° deflectors follow a new design[23] that provides control of the ion beam focusing in both dimensions, unlike traditional cylindrical or quadrupole deflectors that create an astigmatic output beam. Our cylindrical deflectors use plates of differing heights to mimic the field of a spherical deflector at the ideal ion beam orbit without the cost and size of a true spherical deflector.

In operation, about 50% of the 10 μA ion beam current that is measured in the Faraday cup in the first ion deflector chamber can be transported through the overlap region and both deflectors and collected in the retractable Faraday cup after deflector 2. But once the 3 mm apertures are put into place in the drift region, only 1–2 μA of beam current make it through the system. After traversing the overlap region, the ion beam is turned by the second deflector, collimated by a second Einzel lens, and directed into the time-of-flight mass spectrometer.

D. Time-of-flight mass spectrometer

1. MS design

The Saykally ion beam instrument used a Wien velocity filter as a mass analyzer to identify the ions present in their beam and to optimize the current of the ion of interest. However, due to the relatively low mass resolution of the Wien filter, this optimization was performed at a lower beam energy than that at which spectroscopy was performed.[17–19]

In contrast, we have adopted a beam modulation[26,27] TOF-MS, which creates an ion packet from our continuous ion beam. This technique can perform mass and energy analysis at full beam energy, thereby avoiding the possibility that the ion beam composition may be dependent on the extraction voltage. Figure 1 shows the TOF-MS region, consisting of an Einzel lens and a pair of vertical electrostatic deflector plates. The deflection plates are held at an equal voltage but with opposite polarity. The polarity of the plates is then quickly reversed to sweep the ion beam over a 3.2 mm diameter aperture located near the detector. Two beam profilers aid in aligning the ion beam through the 1.53 m drift tube and onto the electron multiplier detector. At a beam voltage of 4 kV, our TOF-MS has a measured resolution of $m/\Delta m$ ~ 400, which will be sufficient for optimizing the production of even large molecular ions such as $C_6H_7^+$.

2. MS results

The mass spectrometer is used to (1) identify the ion species in the plasma, (2) estimate the beam energy, and (3) calculate the energy spread of the ions created by the cold cathode plasma source. In a nitrogen plasma under typical conditions, the source produces mostly N_2^+ and N^+ in a ratio of $\sim 10:1$, as shown in Figure 3. The field-free flight tube
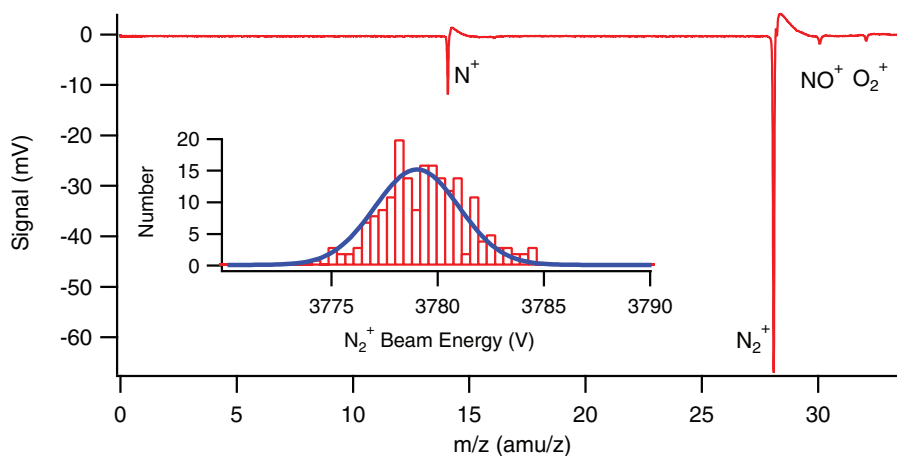

FIG. 3. Mass spectrum of an ion beam formed from a N_2 plasma, showing an N_2^+:N^+ ratio of $\sim 10:1$. The inset shows the energy distribution of the N_2^+ ions.

length combined with arrival times of individual ions can be used to estimate both the average beam energy as well as the energy spread of the ions in the beam, as shown in Figure 3. For a beam voltage of ∼3780 V, the energy spread was found to be 4.7 V (FWHM), which is consistent with the spectroscopic linewidths presented in Sec. III A.

E. Spectroscopy

1. Heterodyne detection

The Ti:Sapphire laser, optical cavity, locking scheme,[7,28] and the NICE-OHMS technique[29] have been described previously, so only a brief overview is given here. Two sets of RF sidebands are added by electro optic modulators (EOM). The first non-resonant EOM adds sidebands at ∼30 MHz with a small modulation index. The signal from a back reflection off of the cavity is demodulated with an RF mixer to generate the Pound-Drever-Hall[30] error signal. An analog lockbox splits corrections from the error signal into slow and fast components. The slow corrections are sent to the cavity piezo to alter the cavity length, while the fast corrections are sent to the voltage controlled oscillator (VCO) that drives the acousto optic modulator (AOM) to make small changes in the laser frequency. As shown in Figure 1, the laser is double passed through an 85 MHz resonant AOM, which makes the pointing of the laser beam immune to changes in the AOM frequency[31] and induces a 170 MHz redshift to the laser light. The second EOM, resonant at 113 MHz, adds sidebands at exactly the free spectral range of the optical cavity with a modulation index $\beta \sim 0.83$. The laser is coupled into the cavity, and the light transmitted through the cavity is detected with a fast photodiode.

Heterodyne spectroscopy (including NICE-OHMS) is sensitive to both absorption and dispersion signals, which when unsaturated[32] are related to one another through the Kramers-Kronig relations. Since the two signals appear 90° out of phase with one another with respect to the RF modulation, it is possible to independently observe each signal with phase sensitive detection. To take advantage of this aspect of the spectroscopy, the AC component of the detector signal is amplified, split into two paths, and demodulated with two separate mixers which are set to be 90° out of phase with one another. The overall detection phase is adjusted using an RF phase shifter in the line between the RF generator and the amplifier that drives the 113 MHz EOM. The RF phase shifter is used to set one mixer to record solely the dispersion phase.

2. Modulation scheme and Doppler splittings

Because residual amplitude modulation induced by the EOM or external etalons can limit the sensitivity of NICE-OHMS, it is advantageous to use a second form of modulation.[34] In this work, the velocity of the ions is modulated by a square wave voltage at 4 kHz applied to the drift tube and aperture plates. After the heterodyne RF signal is demodulated with the mixers, the velocity modulation signal is demodulated using the lock-in amplifiers.

Because the laser propagates both parallel and anti-parallel to the fast ion beam, each spectral line is both red (−) and blue (+) Doppler shifted away from the rest frequency (ν_0) to

$$\nu_{\pm} = \nu_0 \sqrt{\frac{1 \pm v/c}{1 \mp v/c}}, \tag{1}$$

where the velocity of the ions $v = \sqrt{2qV'/M}$, q is the charge of an electron, V' is the voltage of the ion beam in the drift tube, and M is the mass of the species. The voltage of the ion beam in the drift tube V' is determined from the modulation voltage (V_{mod}) by $V' = V_{beam} \pm V_{mod}$. (Note that the typical approximation $\nu_{\pm} \sim \nu_0(1 \pm v/c)$ is inaccurate by ∼50 MHz at this frequency.) In a case where multiple ions are present, this Doppler splitting will provide mass identification of every spectral line.

For example, the red and blue components of a 1.985 kV ion beam of N_2^+ are separated by ∼254 GHz (∼8.47 cm^{-1}). With a 2 V$_{pp}$ square wave driving the velocity modulation, the red and blue components are Doppler split again into components separated by 128 MHz. This splitting is not resolved, given the residual Doppler linewidth (observed to be 90 MHz for the ∼2 kV beam) and the 113 MHz sideband spacing.

3. Frequency comb calibration

For ultra-high accuracy and precision on the frequency measurements, an erbium doped fiber amplifier frequency comb (MenloSystems FC1500/0060) is used to precisely calibrate the frequency of our Ti:Sapphire laser. For each point in our spectrum, the frequency of the Ti:Sapphire laser is determined by measuring the beat frequency between the Ti:Sapphire laser and the nearest comb mode.[28,29] In order to demonstrate the precision of the spectroscopic measurements, several frequency comb calibrated scans are shown in Sec. III A. The line center for the red Doppler shifted (ν_-) and the blue Doppler shifted (ν_+) components are measured by averaging scans of each component taken with both increasing and decreasing laser frequency, in order to compensate for apparent frequency shifts caused by the finite time constant of the lock-in amplifier. (Our scanning rate corresponds to only ∼12 time constants from the minimum to the maximum of the dispersion profile, whereas a wait time of 10 time constants would be needed for the lock-in to reach 99% of its final value at the presently used 24 dB/octave roll-off.) As can be seen from Eq. (1), the rest frequency can then be determined as the geometric mean of the frequencies of the red- and blueshifted components, $\nu_0 = \sqrt{\nu_- \nu_+}$.

III. RESULTS

A. Spectroscopic results

Two typical scans of the Q$_{22}$(14.5) line of the 1-0 band of the $A^2\Pi_u - X^2\Sigma_g^+$ Meinel system of N_2^+ are shown in Figure 4. Only the dispersion phase is displayed, because no signal was observed at the absorption detection phase due to optical saturation, as described below.
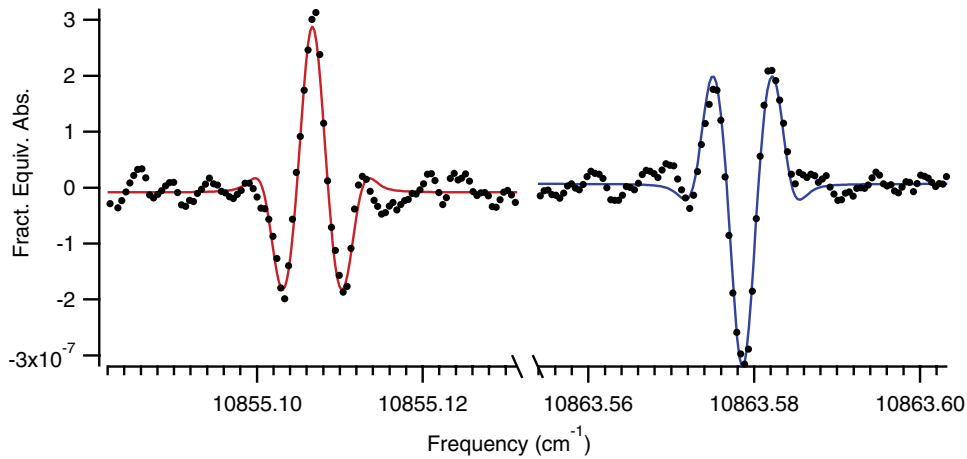
FIG. 4. Scans of red- and blue-shifted components of the Q$_{22}$(14.5) line (black dots) collected at 1.985 kV beam voltage along with fits to Eq. (3) (solid curves). For clarity, only 1 in every 15 experimental points is shown. The Doppler shifted lines are 180° out of phase with one another, allowing for identification of the sign of a component's Doppler shift. The Doppler shifted components are separated by ∼8.5 cm^{-1} as expected from Eq. (1). See the supplementary material[33] for more information about the vertical scale.

The line shape function for a dispersion signal for NICE-OHMS is given by[34]

$$\chi_{n-o}^{disp}(\nu_d) = \chi^{disp}(\nu_d - \nu_{fm}) - 2\chi^{disp}(\nu_d) \quad (2)$$
$$+ \chi^{disp}(\nu_d + \nu_{fm}),$$

where χ^{disp} is the general dispersion line shape function, ν_d is the de-tuning ($\nu_d = \nu - \nu_0$) of the carrier from the center frequency (ν_0) of the transition, and ν_{fm} is the RF modulation frequency (113 MHz).

The velocity modulation induces a second Doppler splitting (ν_{vm}) where the positive and negative splitting are 180° out of phase with one another. Therefore, the line shape for a dispersion signal for a NICE-OHMS velocity modulated ion beam signal is

$$\chi_{vm}^{disp}(\nu_d) = \chi_{n-o}^{disp}(\nu_d - \nu_{vm}) - \chi_{n-o}^{disp}(\nu_d + \nu_{vm}). \quad (3)$$

The Gaussian dispersion line shape, derived from a peak-normalized Gaussian line shape, is given by[32,35]

$$\chi^{disp}(\nu_d) = -\frac{2}{\sqrt{\pi}} e^{-\gamma^2} \int_0^\gamma e^{\gamma'^2} d\gamma', \quad (4)$$

where $\gamma = 2\nu_d \sqrt{\ln 2}/\Delta\nu$ and $\Delta\nu$ is the FWHM for the Gaussian profile.

When the spectra are fit to Eq. (3), the line center, FWHM, and peak-normalized Gaussian amplitude are obtained. An example of the red- and blue-shifted components of a NICE-OHMS signal are shown in Figure 4. The average linewidth for a 4 kV beam was ∼120 MHz, which is consistent with the beam energy spread observed with the TOF-MS. Some slight asymmetry is seen between the amplitudes of the positive and negative velocity modulation components, and appears to be dependent on the alignment and overlap of the ion beam with the laser beam, which we have not yet fully optimized. We expect to have more useful diagnostic information regarding this asymmetry when we move to mid-infrared spectroscopy, as the narrower linewidth will enable

a full resolution of the heterodyne and velocity modulation splittings.

Figure 5 shows an example of how spectra calibrated with the frequency comb are used to determine the line center. For each red- and blueshifted component of the NICE-OHMS signal, scans in opposite directions were collected, as described above. The average of the blue-shifted transitions was $\nu_+ = 10865.19163$ cm^{-1} and the average of the red-shifted transitions was found to be $\nu_- = 10\,853.49936$ cm^{-1}. The geometric mean of these two values gives a rest transition frequency of $\nu_0 = 10859.34392$ cm^{-1}, which is within 8 MHz of the rest frequency of 10859.34418 cm^{-1} measured with sub-Doppler resolution and frequency comb calibration in a positive column discharge.[29] This accuracy appears to be limited primarily by the asymmetry in the observed line-shapes (the optical frequency comb itself has an accuracy ≪1 MHz), and so we expect this to be further improved in the future.
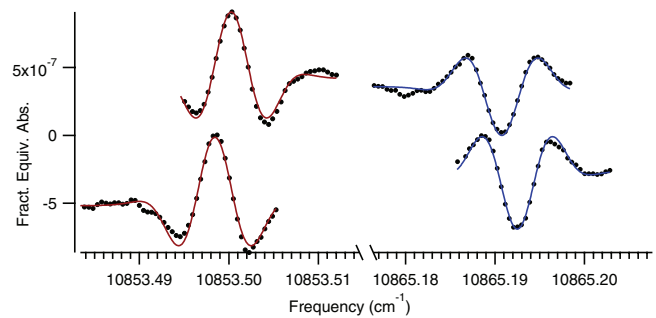

FIG. 5. Scans of red- and blue-shifted components of the Q$_{22}$(14.5) line (black dots) collected at 3.781 kV beam voltage along with fits to Eq. (3) (solid curves) where the frequency axis is calibrated with the frequency comb. For clarity, only 1 in every 15 experimental points is shown. The top two traces are scanned toward the rest frequency and the bottom are scanned away from the rest frequency. As discussed in the text, the apparent frequency shifts are artifacts of the lock-in detection. The spectra have been offset vertically for clarity.

B. Sensitivity and saturation

For a baseline scan obtained with a 3 s lock-in time constant (and a 24 dB/octave roll-off, with a resulting detection bandwidth of 0.03 Hz), the observed noise equivalent absorption is $\sim 2 \times 10^{-11}$ cm^{-1} Hz$^{-1/2}$, which is a factor of 50 lower than the Saykally ion beam instrument.[17] The improvement comes from several factors: a lower fractional noise level at the detector (1.3×10^{-8} vs. 2×10^{-7}), thanks in part to heterodyne detection; a higher cavity finesse ($\mathcal{F}$, 450 vs. 100); and a longer laser/ion overlap length (L, 27 cm vs. 15 cm).

The shot noise limit for the instrument is given by[36]

$$\sigma_{\text{shot noise}} = \frac{\pi}{\mathcal{F} \times L} \sqrt{\frac{qB}{\eta P_0}} \frac{1}{J_0(\beta) J_1(\beta)}, \qquad (5)$$

where q is the charge of an electron, B is the bandwidth of detection, η is the detector responsivity, P_0 is the power incident on the detector, and $J_n(\beta)$ are Bessel functions of the heterodyne modulation index, β. The effective path length through the ion beam is the laser/ion beam interaction length ($L = 27$ cm) times the number of round trip passes ($\mathcal{F}/\pi$). At a typical power level (incident on the detector) of 1.10 mW, the expected fractional shot noise is $\sim 2 \times 10^{-12}$ cm^{-1}. Thus, the observed noise in the instrument ($\sim 3 \times 10^{-12}$ cm^{-1}) is within a factor of ~ 1.5 of the shot noise limit.

Absorption signals are not observable in this experiment due to the high degree of optical saturation, which is due to the high intracavity laser power and the lack of any relaxation process for the ions in the beam. For typical experimental conditions, we estimate the saturation parameter[32] of $G_0 \sim 30000$ for the carrier and $G_1 \sim 6300$ for the sidebands. The absorption signal should be reduced by a factor of $\sqrt{1+G_1} \sim 80$, and is not detectable given our signal-to-noise ratio.

The impact of saturation on the dispersion signal in NICE-OHMS is strongly dependent on the ratio between the homogenous linewidth in the absence of saturation and the Doppler width (this ratio is denoted y in Ref. 32). Assuming the homogenous linewidth is set by the transit time ($\sim 1.6\ \mu$s for a 4 kV beam), and that the Doppler width is 120 MHz (from our fits), we expect $y \sim 0.0038$, and the dispersion signal should be reduced by only a factor of ~ 2 at these saturation parameters.

However, the observed dispersion signals are a factor of ~ 6 weaker than would be expected based on the ion number density, the transition strength, and the signal reduction from saturation, as described in the supplementary material.[33] At present, we can only speculate as to the reason for this discrepancy; possible reasons include: (1) not all N_2^+ ions may be in the vibronic ground state, (2) the actual Doppler-width may be narrower than the observed width if the latter has contributions from jitter in the beam energy caused by the power supplies, and (3) the overlap between the ion beam and the laser beam may be imperfect (as suggested by the asymmetries in the lines). We anticipate that future experiments in the mid-infrared will shed further light on this discrepancy.
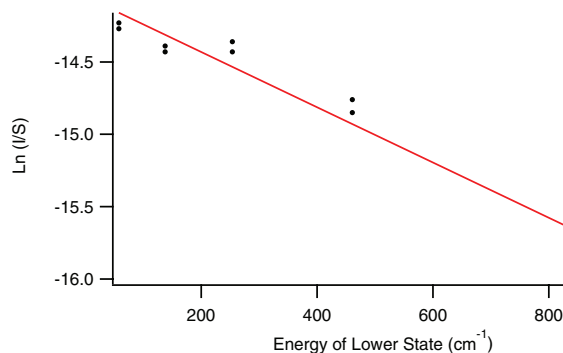

FIG. 6. Boltzmann diagram for observed N_2^+ transitions; for each transition, a separate measurement is shown for each of the red- and blue-shifted components to illustrate the reproducibility of the intensities. The calculated rotational temperature is 753 ± 45 K.

C. Discussion

In order to characterize the rotational distribution of the N_2^+ ions produced by our ion source, spectra of the $^qQ_{22}(J)$ lines (with $J = 4.5, 7.5, 10.5, 14.5,$ and 21.5) with lower energies ranging from 60 to 970 cm^{-1} were collected. The spectra were fit to Eq. (3). The observed intensities (I) were normalized to the strength (S) of the transition, which was obtained along with the lower state energies from PGOPHER[37] using constants from Ref. 22. Figure 6 shows a Boltzmann diagram for the five observed transitions. From the slope of the linear regression fit, the rotational temperature is 753 ± 45 K.

While we only observed several transitions, this highly resolved technique could easily be applied to the observation of tens or hundreds of transitions. As the previous work[22] observed Doppler-limited transitions with linewidths of 1-1.4 GHz, the line centers were only determined to a precision around 60 MHz, with an accuracy of 150 MHz. With modest improvements to our current system, the accuracy of line center determination could be improved by at least a factor of 50 compared to the Doppler-limited measurements. This would greatly improve the overall RMS of the current effective Hamiltonian fit (RMS ~ 100 MHz) and the individual observed–calculated values for many blended lines.

Finally, it should be noted that ion beam spectra enjoy a completely rigorous ion/neutral discrimination, both from the spatial separation of the ions from the neutrals and from the velocity modulation. While our previous cavity-enhanced velocity modulation technique studies[7,28,29] showed a discrimination between ions and neutrals in the lock-in detection phase, the ion beam technique is rigorously insensitive to absorbing or dispersing neutrals.

IV. CONCLUSIONS AND FUTURE DIRECTIONS

We have demonstrated the construction of a fast ion beam spectrometer which provides rigorous spatial and velocity modulation discrimination against neutral signals. We have demonstrated the instrument's capabilities by showing narrow (~ 120 MHz) spectral lines from the $A^2\Pi_u - X^2\Sigma_g^+$

system of N_2^+; this represents the first direct spectroscopy of an electronic transition in an ion beam. The ion beam instrument has a high-resolution mass spectrometer that provides online mass spectra at spectroscopically relevant beam energies. The dispersion line shape of the NICE-OHMS signal has been described, as well as the sensitivity and the observed noise. With the current detectors and laser power, the noise is close to the shot noise limit. The NICE-OHMS instrument reported in this article has been shown to be a factor of 50 more sensitive than the previous direct absorption ion beam instrument.[17] The rotational temperature of ions in the ion beam was found to be ~750 K.

The laser spectroscopy reported here was based on using two EOMs on a frequency tunable Ti:Sapphire laser. By combining the output of this Ti:Sapphire with a cw Nd:YAG laser in a periodically poled lithium niobate crystal, a mid-IR laser with appropriate sidebands can be generated. This will enable the extension of this NICE-OHMS ion beam spectroscopy technique into the mid-IR to record the fundamental vibrational bands of a wide variety of molecular ions in the 2.8–4.8 μm region.

Finally, it is expected that a continuous supersonic expansion discharge source[20] and skimmer will replace the cold cathode ion source in the near future. The use of a supersonic expansion will enable the spectroscopy of larger and more fluxional molecular ions (e.g., CH_5^+ and $C_3H_3^+$), for which quantum dilution at higher rotational temperatures has complicated previous attempts to apply velocity modulation spectroscopy.

ACKNOWLEDGMENTS

[1] E. E. Ferguson and F. Arnold, Acc. Chem. Res. **14**, 327 (1981).
[2] E. Herbst and W. Klemperer, Astrophys. J. **185**, 505 (1973).
[3] T. Oka and M. F. Jagod, J. Chem. Soc., Faraday Trans. **89**, 2147 (1993).
[4] S. K. Stephenson and R. J. Saykally, Chem. Rev. **105**, 3220 (2005).
[5] C. S. Gudeman, M. H. Begemann, J. Pfaff, and R. J. Saykally, Phys. Rev. Lett. **50**, 727 (1983).
[6] M. F. Jagod, C. M. Gabrys, M. Rosslein, D. Uy, and T. Oka, Can. J. Phys. **72**, 1192 (1994).
[7] B. M. Siller, A. A. Mills, and B. J. McCall, Opt. Lett. **35**, 1266 (2010).
[8] S. Davis, M. Farnik, D. Uy, and D. J. Nesbitt, Chem. Phys. Lett. **344**, 23 (2001).
[9] D. T. Anderson, S. Davis, T. S. Zwier, and D. J. Nesbitt, Chem. Phys. Lett. **258**, 207 (1996).
[10] K. C. Thompson, D. L. Crittenden, and M. J. T. Jordan, J. Am. Chem. Soc. **127**, 4954 (2005).
[11] G. A. Olah, G. Klopman, and R. H. Schlosberg, J. Am. Chem. Soc. **91**, 3261 (1969).
[12] E. T. White, J. Tang, and T. Oka, Science **284**, 135 (1999).
[13] C. Savage, F. Dong, and D. J. Nesbitt, paper presented at 61st International Symposium on Molecular Spectroscopy, The Ohio State University, Columbus, OH, 2006.
[14] X. Huang, A. B. McCoy, J. M. Bowman, L. M. Johnson, C. Savage, F. Dong, and D. J. Nesbitt, Science **311**, 60 (2006).
[15] D. J. Nesbitt, paper presented at the 8th International Conference of Computational Methods in Sciences and Engineering, Kos, Greece, 3 October 2010.
[16] W. H. Wing, G. A. Ruff, W. E. Lamb, Jr., and J. J. Spezeski, Phys. Rev. Lett. **36**, 1488 (1976).
[17] J. V. Coe, J. C. Owrutsky, E. R. Keim, N. V. Agman, D. C. Hovde, and R. J. Saykally, J. Chem. Phys. **90**, 3893 (1989).
[18] J. C. Owrutsky, E. R. Keim, J. V. Coe, and R. J. Saykally, J. Phys. Chem. **93**, 5960 (1989).
[19] E. R. Keim, M. L. Polak, J. C. Owrutsky, J. V. Coe, and R. J. Saykally, J. Chem. Phys. **93**, 3111 (1990).
[20] K. N. Crabtree, C. A. Kauffman, and B. J. McCall, Rev. Sci. Instrum. **81**, 086103 (2010).
[21] J. Ye, L. S. Ma, and J. L. Hall, J. Opt. Soc. Am. B **15**, 6 (1998).
[22] D. W. Ferguson, K. N. Rao, P. A. Martin, and G. Guelachvili, J. Mol. Spectrosc. **153**, 599 (1992).
[23] H. Kreckel, H. Bruhns, K. A. Miller, E. Wahlin, A. Davis, S. Hockh, and D. W. Savin, Rev. Sci. Instrum. **81**, 063304 (2010).
[24] J. H. Moore, C. C. Davis, and M. A. Coplan, *Building Scientific Apparatus* (Perseus Books, Cambridge, MA, 2002), p. 371.
[25] J. R. Pierce, J. Appl. Phys. **11**, 548 (1940).
[26] J. M. B. Bakker, J. Phys. E **6**, 785 (1973).
[27] J. M. B. Bakker, J. Phys. E **7**, 364 (1974).
[28] A. A. Mills, B. M. Siller, B. J. McCall, Chem. Phys. Lett. **501**, 1 (2010).
[29] B. M. Siller, M. W. Porambo, A. A. Mills, and B. J. McCall, Opt. Express **19**, 24822 (2011).
[30] R. W. P. Drever, J. L. Hall, F. V. Kowalski, J. Hough, G. M. Ford, A. J. Munley, and H. Ward, Appl. Phys. B **31**, 97 (1983).
[31] E. A. Donley, T. P. Heavner, F. Levi, M. O. Tataw, and S. R. Jefferts, Rev. Sci. Instrum. **76**, 063112 (2005).
[32] W. Ma, A. Foltynowicz, and O. Axner, J. Opt. Soc. Am. B **25**, 1144 (2008).
[33] See supplementary material at http://dx.doi.org/10.1063/1.3665925 for details of the calculation of both observed and expected fractional equivalent absorption.
[34] A. Foltynowicz, F. M. Schmidt, W. Ma, and O. Axner, Appl. Phys. B **92**, 313 (2008).
[35] A. Foltynowicz, W. G. Ma, F. M. Schmidt, and O. Axner, J. Opt. Soc. Am. B **25**, 1156 (2008).
[36] J. Ye, "Ultrasensitive high resolution laser spectroscopy and its application to optical frequency standards," Ph.D. dissertation (University of Colorado Department of Physics, 1997).
[37] C. M. Western, PGOPHER, a program for simulating rotational structure, University of Bristol, 2009, see http://pgopher.chm.bris.ac.uk.